Supplementary Material for: "Intracavity spatiotemporal metasurfaces"

Wenhe Jia,[a,†] Chenxin Gao,[a,†] Yongmin Zhao,[b] Liu Li,[a] Shun Wen,[a] Shuai Wang,[a] Chengying Bao,[a,*] Chunping Jiang,[b,*] Changxi Yang,[a] Yuanmu Yang[a,*]

[a] State Key Laboratory of Precision Measurement Technology and Instruments, Department of Precision Instrument, Tsinghua University, Beijing 100084, China
[b] Key Laboratory of Nanodevices and Applications, Suzhou Institute of Nano-Tech and Nano-Bionics, Chinese Academy of Sciences, Suzhou, 215123, China

*Address all correspondence to Yuanmu Yang, E-mail: ymyang@tsinghua.edu.cn; Chunping Jiang, E-mail: cpjiang2008@sinano.ac.cn; Chengying Bao, E-mail: cbao@tsinghua.edu.cn

[†]These authors contributed equally to this work

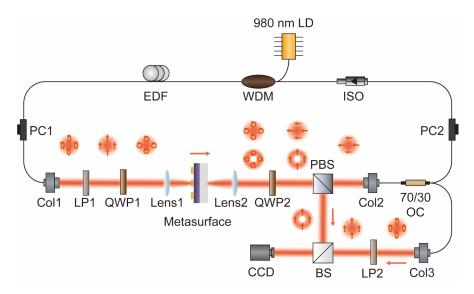## 1   Method for metasurfaces fabrication

The fabrication of the metasurface is done via a commercial service offered by Tianjin H-Chip Technology group. The pattern of the plasmonic antennas is defined using a standard electron beam lithography, evaporation, and lift-off process. The thickness of the gold nano-antenna is 40 nm, with 5-nm-thick titanium used as the adhesive layer. We find that after the metasurface fabrication process, the ENZ wavelength of the ITO film redshifts, which is possibly due to the sample heating during the photoresist baking process. We experimentally find that re-annealing the sample in the N_2 atmosphere at 300 °C for 2 hours can recover the ENZ wavelength of the ITO film to its original state. The size of the polarization-insensitive metasurface and geometric phase metasurfaces are 300×300 μm^2 and 200×200 μm^2, respectively. The geometric phase metasurfaces' unit cell has a period of 700 nm. The rectangular nano-antenna has a length of 350 nm and a width of 210 nm.

2   Experimental setup for the vortex beam generation

The schematic of the experimental setup for the vortex beam generation is shown in Fig. S1. A 980 nm laser diode serves as the pump source. It is coupled into the laser cavity through a 980

nm/1550 nm wavelength-division multiplexer. The laser cavity is composed of a 2-meter-long Er-doped fiber (Nufern SM-ESF-7/125) as the gain medium and a 5.5-meter-long single-mode fiber (YOFC SMF). The net dispersion of the laser cavity is -0.16 ps^2. To minimize the loss of the laser cavity, two polarization controllers are utilized to change the polarization state of the output light from the collimator. A fiber isolator is utilized to maintain unidirectional light propagation in the laser cavity. The focal length of lenses in the free space is 10 mm. The spatial mode profiles of the output vortex beam are measured by an InGaAs camera (Hamamatsu C14041-10U).

To characterize the vortex beams directive coupled out from the polarization beam splitter, we interferent it with the Gaussian beam from the output coupler. Another polarizer is employed to convert the Gaussian beam to the same polarization state as the vortex beam. They are then combined by a beam splitter before being transmitted to the CCD for the measurement of the interference patterns.

Figure S1 Schematic illustration of the experimental setup for the intracavity vortex beam generation measurement. LD, laser diode; EDF, Er-doped fiber; WDM, 980 nm/1550 nm wavelength-division multiplexer; ISO, optical isolator; PC, polarization controller; OC, output coupler; Col, collimator; LP, linear polarizer; QWP, quarter-wave plate; PBS, polarization beam splitter; BS, beam splitter; CCD, charge-coupled device.

3   Method for ITO thin-film growth

The ITO film with 20-nm-thickness is deposited on a glass substrate at room temperature by DC magnetron sputtering with a sintered ceramic target of ITO (In_2O_3/SnO_2 90/10 wt %). Before the deposition, the chamber is evacuated to less than 10^{-3} Pa by a turbo molecular pump. During the sputtering, an ultra-high purity argon gas with a flow rate of 82 sccm is introduced into the chamber, and the working pressure is kept at 0.4 Pa. A DC power of 80 W is applied without intentionally heating the substrate. After the growth, the film is annealed at 750 °C for 10 minutes in N_2 atmosphere to improve its crystallinity. The film is subsequently annealed at 350 °C for 5 minutes in O_2 atmosphere to adjust its ENZ wavelength to 1558 nm.

4   Linear characteristics of the ITO film

The linear optical property of the ITO film is characterized via spectroscopic ellipsometry. Its permittivity follows the Drude model as:[30]

$$\varepsilon(\omega)=\varepsilon_\infty-\frac{\omega_p^2}{\omega^2+i\gamma\omega} \tag{S1}$$

where $\varepsilon_\infty = 4.25$ is the high-frequency permittivity, $\omega_p = 2.51\times10^{15}$ rad/s is the plasma frequency, and $\gamma = 1.32\times10^{14}$ rad/s is the plasma damping rate. The real part of its permittivity crosses zero at 1558 nm, with an imaginary permittivity of 0.46.

5   Error analysis of the linear transmittance of the strongly coupled metasurface

The discrepancy between the simulated and experimentally measured results is likely due to the difference in the geometry parameters of the simulated and fabricated metasurfaces, as well as the inaccuracy of the fitted refractive index of the ITO film. As shown in Fig. S2, we simulate the transmittance of the metasurface with respect to the radius of the circular nano-antenna and the

plasma frequency ω_p of the ITO film. While the strongly-coupled ENZ-metasurface system has two resonance dips, the radius of the circular nano-antenna has a greater impact on the short-wavelength resonance, while the plasma frequency of the ITO film has a greater effect on the long-wavelength resonance.
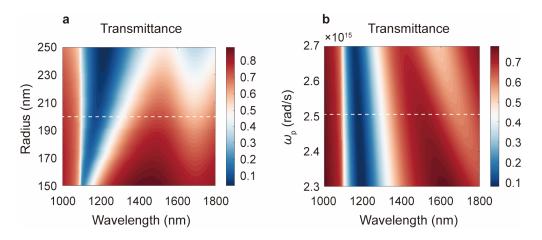

Figure S2 Analysis of the discrepancy between simulated and experimentally measured transmittance of the strongly coupled metasurface. (a)-(b) Simulated transmittance of the strongly coupled metasurface with respect to the radius of the nano-antenna (a) and the plasma frequency ω_p of the ITO film (b), respectively. The simulation parameters used in the main text are labeled by white dashed lines.

6   Nonlinear calculations of the strongly coupled metasurfaces based on the hot-electron model

The giant nonlinear saturable absorption of the strongly coupled system is attributed to the ITO film's large optical nonlinearity, which is further amplified by the plasmonic metasurface. To quantify the system's nonlinear optical properties, we first investigate the nonlinear response of ITO film using the hot-electron model. The non-parabolic shape of the ITO film's conduction band is responsible for its large nonlinearity near its ENZ wavelength, which can be described by Kane's model as:[39]

$$\frac{\hbar^2 k^2}{2m_0^*} = E + CE^2 \tag{S2}$$

where $\hbar$ is the reduced Planck's constant, k is the electron momentum, m_0^* is the effective mass of electrons at the conduction band minimum (CBM), E is the electron energy as a function of the CBM, and C is a coefficient that characterizes the non-parabolicity of the conduction band.

The linearized collisionless Boltzmann equations are used to calculate the relationships between the electron density N_e, the electron energy density U, and ω_p of the ITO film as:[39]

$$N_e(\mu_c, T_e) = \frac{1}{\pi^2} \int_0^\infty dE \frac{m_0^*}{\hbar^2}(1+2CE)(\frac{2m_0^*}{\hbar^2}(E+CE^2))^{\frac{1}{2}} f_0(\mu_c, T_e) \tag{S3}$$

$$U(\mu_c, T_e) = \frac{1}{\pi^2} \int_0^\infty dE \frac{m_0^*}{\hbar^2}E(1+2CE)(\frac{2m_0^*}{\hbar^2}(E+CE^2))^{\frac{1}{2}} f_0(\mu_c, T_e) \tag{S4}$$
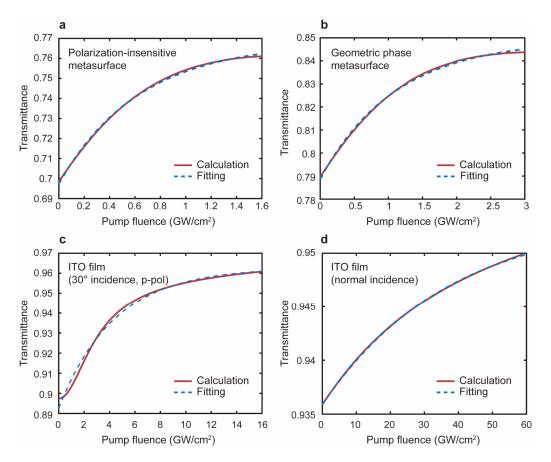
$$\omega_p(\mu_c, T_e)^2 = \frac{e^2}{3m_0^*\pi^2\varepsilon_0} \int_0^\infty dE (\frac{2m_0^*}{\hbar^2}(E+CE^2))^{\frac{3}{2}}(1+2CE)^{-1}(-\frac{\partial f_0(\mu_c, T_e)}{\partial E}) \tag{S5}$$

where μ_c is the electron chemical potential, T_e is the electron temperature, and f_0 (μ_c, T_e) is the Fermi-Dirac distribution. For the following calculation, $m_0^* = 0.263m_0$ and $C = 0.4191$ eV^{-1} are utilized,[65] where m_0 is the free electron mass. We first obtain N_e with a static ω_p ($T_e = 300$ K) based on Equation S3 and Equation S5. Note that N_e is a constant because all free electrons remain in the conduction band of ITO under photo-excitation. Subsequently, we could obtain μ_c, U, and ω_p with respect to T_e using Equations S3-S5, respectively.

Next, the transmittance T and absorption A of the strongly coupled system as a function of ω_p of the ITO film are calculated by the commercial software Lumerical FDTD Solutions. The relationship between the pump fluence F and U could then be determined as:

$$F = \left(U\left(T_e\right) - U(300K)\right) / A_0 \tag{S6}$$

where A_0 is the absorption of the strongly coupled metasurfaces with static ω_p. Finally, we obtain the saturable absorption curves of the polarization-insensitive and the geometric phase metasurface, as shown in Fig. S3a and Fig. S3b, respectively. Using Equation 3 of the main text, the fitted saturable fluence from the theoretical model is 0.63 GW/cm^2 and 1.10 GW/cm^2 for the polarization-insensitive metasurface and the geometric phase metasurface, respectively. The saturable absorption curves of a bare 20-nm-thick ITO film at oblique and normal incidence are also calculated, as shown in Fig. S3c and Fig. S3d, respectively. The linear optical properties of the bare ITO film are calculated by the transfer matrix method.[66] Table S1 summarizes the fitting parameters, indicating that the saturable fluences of the strongly coupled metasurfaces are much lower than those of the bare ITO film.
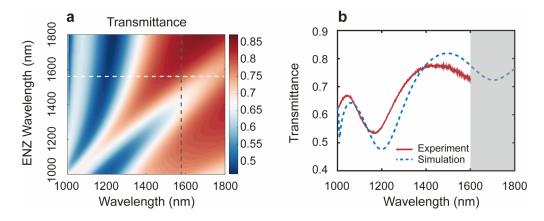
Figure S3 Calculated nonlinear transmittance of the strongly coupled metasurfaces and a bare ITO film. (a)-(b) Calculated (solid line) and fitted (dashed line) pump fluence-dependent transmittance for the polarization-insensitive metasurface (a) and the geometric phase metasurface (b), respectively. (c)-(d) Calculated (solid line) and fitted (dashed line) pump fluence-dependent transmittance for the bare ITO film at an incidence angle of 30° under p-polarization (c) and at normal incidence (d), respectively.

	I_{sat} (GW/cm^2)	A	A_{ns}
Polarization-insensitive metasurface	0.63	7.1%	23.2%
Geometric phase metasurface	1.10	6.0%	15.1%
20-nm-thick ITO film (30° incidence, p-polarization)	4.37	7.0%	3.7%
20-nm-thick ITO film (normal incidence)	37.80	1.8%	4.7%

Table S1 Fitted saturable absorption properties of the strongly coupled metasurfaces and a bare ITO film calculated from the theoretical model, where I_{sat} is the saturable fluence, A is the modulation depth, and A_{ns} is the unsaturable loss.
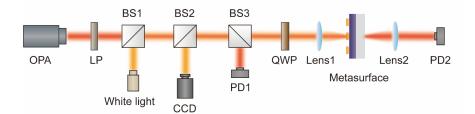
7   Characteristics of the strongly coupled geometric phase metasurface

Figure S4a depicts the simulated linear transmittance of the geometric phase metasurface as a function of the ENZ wavelength of the ITO film with circularly-polarized light incidence. The anti-crossing line shape indicates the strong coupling between the gold nano-antenna and the ITO film.[47] The experimentally measured transmittance, as shown in Fig. 3(d), is in agreement with the simulated result.
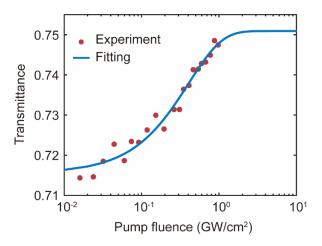
Figure S4 Linear transmittance of the strongly coupled geometric phase metasurface. (a) Simulated transmittance of the geometric phase metasurface as a function of the ENZ wavelength of the ITO film. The static ENZ wavelength of the ITO film is marked by the white dashed line. The laser operation wavelength is indicated by the gray dashed line. (b) Measured (red) and simulated (blue) linear transmittance of the geometric phase metasurface. The gray region denotes the wavelength range where experimental results are not achievable due to the low quantum efficiency of the spectrometer.

To experimentally characterize the saturable absorption properties of the strongly coupled metasurfaces, we build a nonlinear transmittance measurement setup as schematically shown in Fig. S5. The light source is an optical parametric amplifier (Light Conversion Orpheus-ONE-HP) pumped by a Yb: KGW laser oscillator (Light Conversion Pharos). The output laser has a pulse duration of 300 fs and a repetition rate of 75 kHz, with a tunable wavelength in the near-infrared range. A lens with a focal length of 25.4 mm is used to focus light on the metasurface. To determine the transmittance of the metasurface under different pump fluences, we use a pair of photo-detectors (Thorlabs DET10D/M and Thorlabs DET10N/M) to measure the average power of the incident and transmitted beam. To improve the signal-to-noise ratio (SNR) of the measurement, a chopper is utilized in combination with a lock-in amplifier (Zurich Instrument MLFI 500 kHz).

Figure S5 Schematic illustration of the experimental setup for the nonlinear transmittance measurement. OPA, optical parametric amplifier; LP, linear polarizer; QWP, quarter-wave plate; BS, beam splitter; CCD, charge-coupled device; PD, photo-detector.

The measured transmittance of the geometric phase metasurface as a function of pump fluence is shown in Fig. S6. Using Equation 3 of the main text, the fitted saturable fluence of the geometric phase metasurface is 0.41 GW/cm^2.

Figure S6 Nonlinear characterization of the strongly coupled geometric phase metasurface. Measured (dots) and fitted (line) pump fluence-dependent transmittance for the strongly coupled geometric phase metasurface at the operation wavelength of 1580 nm. The fitted parameters are I_{sat} = 0.41 GW/cm^2, A = 3.5%, and A_{ns} = 24.9%, where I_{sat} is the saturable fluence, A is the modulation depth, and A_{ns} is the unsaturable loss.

We compare the saturable absorption properties of both polarization-insensitive metasurface and geometric phase metasurface, with the fitting parameters summarized in Table S2. The

polarization-insensitive metasurface has a relatively higher modulation depth, saturable fluence, and unsaturable loss in comparison with the geometric phase metasurface, which is likely due to the slight differences in the resonance quality factor and the operating wavelength of these two metasurfaces.
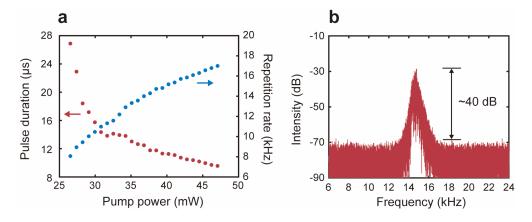
	I_{sat} (GW/cm^2)	A	A_{ns}
Polarization-insensitive metasurface	0.52	7.2%	34.5%
Geometric phase metasurface	0.41	3.5%	24.9%

Table S2 Fitted saturable absorption properties of the polarization-insensitive metasurface and geometric phase metasurface, where I_{sat} is the saturable fluence, A is the modulation depth, and A_{ns} is the unsaturable loss.

8   Characteristics of the Q-switched beams

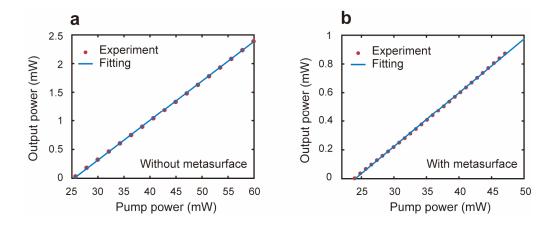*8.1 Pulse duration, repetition rate, and stability of the Q-switched beams*

To characterize the properties of the Q-switched Gaussian beams generated by the polarization-insensitive metasurface, we measure the pulse duration and repetition rate with respect to the pump power, as shown in Fig. S7a. A higher pump power can activate the saturable absorption of the strongly coupled metasurface in less time, resulting in a shorter pulse duration and a higher repetition rate. The stability of the Q-switched beam generation is quantified by the radio-frequency (RF) spectrum, as shown in Fig. S7b. With a pump power of 39 mW, the signal-to-noise ratio (SNR) is 40 dB, and the repetition rate is 14.7 kHz.

Figure S7 Additional characterization of the Q-switched Gaussian beams generated by the polarization-insensitive metasurface. (a) Pump power dependence of the pulse duration (red dots) and repetition rate (blue dots) of the Q-switched beams generated by the polarization-insensitive metasurface. (b) RF spectrum of the Q-switched beam with a pump power of 39 mW. The SNR is 40 dB, with a repetition rate of 14.7 kHz.

8.2 Slope efficiency of the Q-switched beams

The slope efficiencies of the laser cavity for Q-switched pulses generation without and with the polarization-insensitive metasurface are measured, respectively, as shown in Fig. S8. The threshold pump power of continuous-wave beam generation and Q-switched beam generation is 25 mW, and the slope efficiencies for these two cavities are 6.9% and 3.8%, respectively. The decrease in the slope efficiency after the insertion of the metasurface is attributed to the loss induced by the metasurface.

Figure S8 Slope efficiency of the Q-switched beams. (a)-(b) Measured pump power dependence of the laser output power (red dots) of the Q-switched beam without (a) and with (b) the metasurface. The output power scales linearly with the pump power, with fitted slope efficiencies (blue lines) of 6.9% and 3.8%, respectively.

9   Characteristics of the vortex Q-switched beams

9.1 Pulse duration, repetition rate, and stability of the vortex Q-switched beams

The properties of the Q-switched vortex beams generated by the geometric phase metasurface are investigated using the same method. Figure S9a depicts the pulse duration and repetition rate of the Q-switched vortex beam with respect to the pump power. The RF spectrum of the Q-switched vortex beam is measured at a pump power of 51 mW, resulting in an SNR of 47 dB and a repetition rate of 13.8 kHz**,** as shown in Fig. S9b**.**
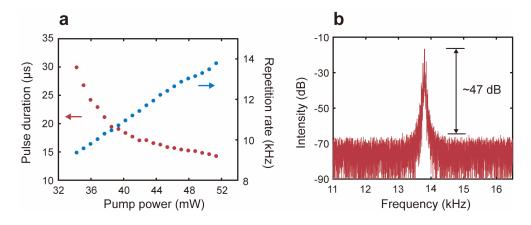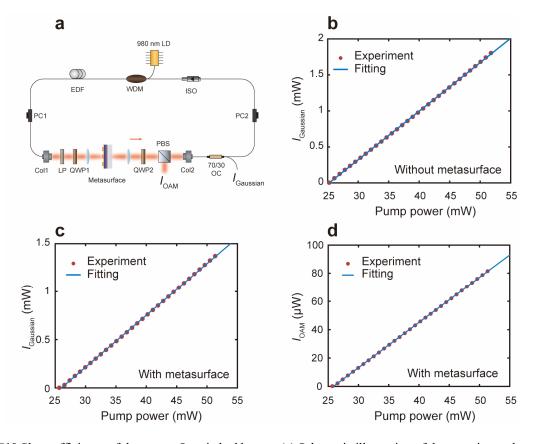
Figure S9 Additional characterization of the Q-switched vortex beams generated by the geometric phase metasurface. (a) Pump power dependence of the pulse duration (red dots) and repetition rate (blue dots) of the Q-switched vortex beams ($l = 2$) generated by the geometric phase metasurface. (b) RF spectrum of the Q-switched vortex beam ($l = 2$) with a pump power of 51 mW. The SNR is 47 dB, with a repetition rate of 13.8 kHz.

9.2 Slope efficiency of the vortex Q-switched beams

We also investigate the slope efficiencies of the laser cavity for the Q-switched vortex pulse generation without and with the geometric phase metasurface. As schematically illustrated in Fig. S10a, the output power of the Gaussian beam $I_{Gaussian}$ from the output coupler (OC) and the output power of the Q-switched vortex beam I_{OAM} from the polarization beam splitter (PBS) are both measured. The slope efficiency of the laser is 6.7% without the geometric phase metasurface, as shown in Fig. S10b. The slope efficiency is slightly lower than that in Fig. S8a, which is due to the loss induced by the linear polarizer (LP). After inserting the metasurface into the laser cavity, the slope efficiency drops to 5.4%, as shown in Fig. S10c. The decrease in slope efficiency is also attributed to the metasurface's loss. As demonstrated in Fig. S10d, the slope efficiency of the Q-switched vortex beam generation is 0.32%. Depending on the polarization conversion efficiency of the geometric phase metasurface, the output coupling energy from the PBS is lower than that

13

from the 70/30 output coupler. The threshold pump powers for the continuous-wave beam generation and the Q-switched pulses generation are 26 mW and 33 mW, respectively.

Figure S10 Slope efficiency of the vortex Q-switched beams. (a) Schematic illustration of the experimental setup for the intracavity vortex beam generation measurement. (b)-(c) Pump power dependence of the output power of the Gaussian beam I_{Gaussian} (red dots) without (b) and with (c) the metasurface, respectively. The fitted slope efficiencies (blue lines) are 6.7% and 5.4%, respectively. (d) Pump power dependence of the output power of the vortex beam I_{OAM} (red dots). The fitted slope efficiency (blue lines) is 0.32% ($l = 2$).

The temporal trace of the output laser beam is measured by a photodetector (Thorlabs DET08CFC) and a 1 GHz real-time oscilloscope (Rigol MSO8104). The spectrum is measured by an optical spectrum analyzer (Agilent 86142B) with a resolution of 0.07 nm. A radio-frequency spectrum analyzer (Agilent N9020A) is utilized to characterize the repetition rate of the pulse train.

The spatial mode profiles of the output vortex beam are measured by an InGaAs camera (Hamamatsu C14041-10U).

10 Contribution analysis of the nonlinear optical response of the strongly coupled system
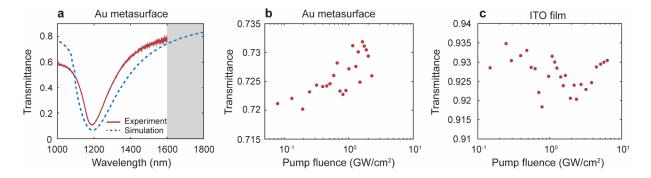
To clarify the contributions of ENZ film and Au metasurface to the nonlinear optical response (NLO) of the strongly coupled system, we performed additional experiments as follows:

First, we anneal the polarization-insensitive metasurface sample in air at 300 °C for 30 minutes to redshift its ENZ wavelength to above 1700 nm. In such a way, the NLO contribution of the ITO film may be minimized. From the measured transmittance of the annealed sample, shown in Fig. S11a, the strong coupling effect disappears. The measured transmittance closely matches the simulated transmittance of an Au metasurface in the absence of the ITO film. Subsequently, we measure the pump fluence-dependent transmittance of the annealed sample, and observe no significant saturable absorption effect at an operation wavelength of 1565 nm (Fig. S11b). After inserting the Au metasurface into the laser cavity, Q-switched pulses could not be generated, indicating that the Au metasurface alone does not exhibit an obvious NLO response at an off-resonance wavelength.

In addition, we also measure the pump fluence-dependent transmittance of a bare ITO film near its ENZ wavelength of 1565 nm under normal incidence, and also do not observe an obvious NLO response, as shown in Fig. S11c. The NLO response of the ITO film could only be boosted with oblique incident light with p-polarization near its ENZ wavelength[30].

With the aid of the Au metasurface, the ENZ mode of the ITO film can be excited by normal incident light. The strongly coupled system can achieve a greater NLO response[47]. As illustrated in Fig. 3e in the main text, the field intensity is amplified and concentrated in the ITO film. The

ITO film may have a greater impact on the NLO response, yet the Au metasurface and the ITO film can complement each other.

Figure S11 Analysis of the contributions of ENZ film and Au metasurface to the nonlinear optical response of the strongly coupled system. (a) Measured (red) and simulated (blue) linear transmittance of the annealed Au metasurface. The gray region denotes the wavelength range where experimental results are not achievable due to the low quantum efficiency of the spectrometer. (b) Measured pump fluence-dependent transmittance of the annealed Au metasurface at the wavelength of 1565 nm. (c) Measured pump fluence-dependent transmittance of the ITO film before annealing at the wavelength of 1565 nm.

11   Polarization-selective effect analysis of the geometric phase metasurfaces for the Q-switching process

A polarizer and a quarter-wave plate are used to fix the polarization state of the light impinging on the geometric phase metasurfaces to be circular. As a result, the metasurfaces have no polarization-selective effect on the incident pulse. A comparative experiment is conducted to further exclude the polarization-selective effect of the geometric phase metasurfaces for the Q-switching process. When the laser works in the Q-switching mode, the geometric phase metasurfaces are moved away from the focus of the lens, resulting in the laser operation transitioning to the continuous-wave mode. The polarization-sensitive elements remain unchanged throughout this process, whereas only the pump fluence of the metasurfaces decreases, indicating that the Q-switching process is induced by the metasurfaces' saturable absorption.